A Numerical Model for Ceiling Flame Spread beneath a Combustible Board with Charring Material

WENGUO WENG and YUJI HASEMI
Department of Architecture, Waseda University
Okubo 3-4-1, Shinjuku-ku
Tokyo, 169-8555, Japan

ABSTRACT

In this paper, an approach for modeling ceiling flame spread beneath a combustible board is developed. The presented model consists of a one-dimensional flame spread model coupled with a one-dimensional pyrolysis model. Firstly, the pyrolysis model is validated against the experimental data from the literature. In addition, the existing experimental data (the ceiling flame spread beneath medium density fibreboard (MDF)) are used for comparison to validate the numerical model. The results obtained from numerical simulations using the presented model are consistent with the experimental tests.

KEY WORDS: ceiling flame spread, charring material, pyrolysis

INTRODUCTION

Flame development under a ceiling is very often the direct trigger for the occurrence of flashover. One of important reasons resulting in the destructive Daegu underground railway fire is the flame spread under the ceiling of carriage [1]. In spite of the importance of ceiling flame for fire safety, there are few fundamental studies related to it. If a ceiling is decorated with combustible materials, it may spread when fire source on the floor is intense enough to ignite directly the ceiling, and a fire of a plain wall or in a wall corner may result in the ceiling flame spread. Such differences of fire scenarios may influence the behavior of ceiling flame itself; horizontal flame under ceiling, the main driving force of the flame spread along the ceiling, may result from the interaction of ceiling flame and other burning objects by which the ceiling is ignited. For the prediction of the ceiling flame spread in these different fire scenarios, it is important to model a pure ceiling flame spread, i.e., flame spread beneath the ceiling starting from an ignition source on the ceiling, as the substantial process of fire growth beneath a ceiling in any scenario. Hasemi and Yokobayashi carried out experiments for study on one-dimensional ceiling flame characteristics, i.e., heat transfer correlation from measurements of flame length and heat flux beneath a noncombustible ceiling surface confined with parallel soffits, and one-dimensional ceiling flame spread beneath medium density fibreboard (MDF) considering the influence of external heating source [2-3]. However, their work is concentrated on the experiments.

Unlike the ceiling fire spread, which has not been paid enough attention to, a great amount of theoretical work of various degrees of complexity has been carried out related

FIRE SAFETY SCIENCE–PROCEEDINGS OF THE EIGHTH INTERNATIONAL SYMPOSIUM, pp. 385-396

to the upward flame spread problem [4-6], another typical concurrent flame spread in fire. In this paper, an approach for modeling the ceiling flame spread beneath a combustible board is developed. The board subjected to a heat flux---when its surface temperature rises above pyrolysis temperature---begins to pyrolyse. The pyrolysis occurs with charring. The “flame spread” is coupled with the pyrolysis of the combustible ceiling in its thickness direction to compute the transient mass flux of the gasified fuel. Thus the presented model consists of a one-dimensional ceiling flame spread model coupled with a one-dimensional pyrolysis model. The ceiling flame spread experimental data from Ref. [2-3] are used for comparison to validate the presented model. In the following section, the model is described in detail. Section 3 discusses the comparisons of the numerical results with experimental data, followed by conclusions.

THE CEILING FLAME SPREAD MODEL

Considering a one-way flame spread beneath the ceiling starting from an ignition source on the ceiling, as shown in Fig. 1, the numerical model calculates the ceiling flame spread by breaking up the surface into a large number of elements. The conditions of each element are independently computed. There are a number of global conditions that are calculated by summing the contributions from each element: the heat release rate, the pyrolysis front and the flame length along the ceiling. Each element is in one of three stages: (1) preheating (above the flame), (2) heating (exposed to the flame), and (3) pyrolysing (burning). The pyrolysis products, volatiles do not accumulate within the material, they migrate without any resistance from the pyrolysis front to the surface which they escape. The gasified fuel burns immediately as it leaves the surface. Thus the stage of pyrolysis is also the stage of burning in this paper. The numerical model keeps track of these conditions for each element.

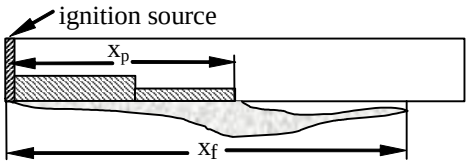

Fig. 1. Schematic of ceiling flame.

Ceiling Flame Length and Heat Fluxes to the Ceiling

Since there are no experimental measurements about heat fluxes to the ceiling in the ceiling flame spread experiments, the correlation for the heat fluxes from flame to the ceiling would be obtained from the experimental data of the heat fluxes from propane line burner to the ceiling, because it has shown that the heat flux to the wall from line fires against the wall and the wall fire itself can be correlated in the same manner [2]. This correlation can be expressed as [2-3]:

$$\dot{q}_f'' = 20 \qquad x/x_f < 0.4$$
$$\dot{q}_f'' = 6.36(x/x_f)^{-1.25} \qquad x/x_f \geq 0.4 \tag{1}$$

where $\dot{q}_f''$ (kW/m^2) is the incident heat flux from the ceiling flame to the ceiling, x (m) is the distance away from the ignition source, and x_f (m) is the ceiling flame length. In the ceiling flame spread experiments [2-3], the ceiling is heated by two sources: (1) an imposed external heat flux, and (2) the incident heat flux from the ceiling flame to the ceiling. Thus, the total heat flux to the ceiling is:

$$\dot{q}'' = \dot{q}_e'' + \dot{q}_f'' \tag{2}$$

Where $\dot{q}''$ (kW/m^2) is the total heat flux to the ceiling, and $\dot{q}_e''$ (kW/m^2) is the imposed external heat flux.

It is obvious that Eq. 1 requires the determination of the flame length. The experimental data from Ref. [2] give the correlations between the flame length and the total heat release rate per unit width as:

$$x_f = 0.096\dot{Q}'^{2/3} \tag{3}$$

Where $\dot{Q}'$ (kW/m) is the total heat release rate per unit width, which is a sum of the contributions of the burner and the burning ceiling material: $\dot{Q}' = \dot{Q}_b' + \dot{Q}_{mat}'$. The contribution of the burner $\dot{Q}_b'$ (kW/m) is known as a priori. The contribution of the burning ceiling material $\dot{Q}_{mat}'$ (kW/m) would be expressed as:

$$\dot{Q}_{mat}' = \chi H_c \sum_{i=1}^{n} \dot{m}_i''(x,t) L_i(x) \tag{4}$$

Where χ is the combustion efficiency, H_c (J/kg) is the heat of combustion of the ceiling material, n is the number of elements which are burning at time t (s), and $L_i(x)$ (m) is the length of the element under consideration. $\dot{m}_i''(x,t)$ (kg/m^{2}s) is the spatially and temporally varying mass loss rate per unit area, which will be given from the pyrolysis model.

The Heat-up Model

This paper adopts the integral models for heat-up [5], which employs an exponential temperature profile across the material, of thickness l (m), and solves the first two moments of the 1-D heat conduction equation. The resulting equations, assuming the material properties k (W/mK) (the thermal conductivity), ρ (kg/m^3) (the density) and c (J/kgK) (the specific heat) constants, are [5]:

$$\frac{d}{dt}[\theta_s \delta(1-e^{-l/\delta})] = \frac{\dot{q}''_{net}}{\rho c} \tag{5}$$

$$\frac{d}{dt}[\theta_s^2 \delta(1-e^{-2l/\delta})] = 4\theta_s \frac{\dot{q}''_{net}}{\rho c} - 4\frac{k}{\rho c}\frac{\theta_s^2}{2\delta}(1-e^{-2l/\delta}) \tag{6}$$

with the initial conditions $\theta_s(t=0)=0$, $\delta(t=0)=0$ (7)

Where $\theta_s = T_s - T_0$ (K) is the surface temperature rise, T_s (K) is the surface temperature, and T_0 (K) is the initial temperature. δ (m) is the thermal penetration depth. $\dot{q}''_{net}$ (kW/m^2) is the net heat flux to the material:

$$\dot{q}''_{net} = \dot{q}'' - \varepsilon\sigma(T_s^4 - T_0^4) - h(T_s - T_0) \tag{8}$$

Where ε and h (W/m^{2}K) are the surface emissivity and convective heat transfer coefficient, respectively. σ (W/m^{2}K^4) is the Stefan-Boltzmann constant.

The Pyrolysis Model

Once an element has reached the pyrolysis temperature T_p (K), it is allowed to pyrolyse, burn, and contribute energy to the ceiling flame. $\dot{m}''_i(x,t)$ in the above section is obtained by this presented pyrolysis model. In the thickness direction of ceiling, a pyrolysis model can be established by assuming: (1) The thermal properties of the material are independent of temperature, (2) The material does not melt or shrink/expand, (3) The moisture content of the material can be ignored, and (4) The pyrolysed gases are assumed to reach the heat surface (do not accumulate within the char layer), which is true from Zicherman *et al.*'s description of the morphology of wood char [7]. Thus, the three-dimensional effects of char pores allow one-dimensional theory to work.

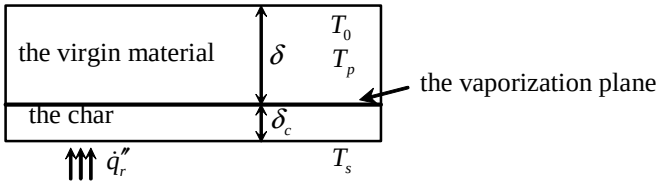

Fig. 2. Schematic of the integral model for the pyrolysis of the charring materials.

The sequence of events occurring in a slab of a solid material when it is exposed to a radiant heat flux can be divided into three distinct phases, shown in Fig. 2, the schematic of the integral model for the pyrolysis of the charring materials: (I) the virgin material, (II) the char and (III) the substrate (not shown in Fig. 2, because nothing of interest happens in that layer). As shown in Fig. 2, the top region is the virgin material. This is the

unreacted material affected by the boundary condition. In this region, the material properties are considered as those of the unreacted material, and the temperature profile is assumed to be parabolic, and considering the boundary condition:

$$T(0,t) = T_p\,,\quad T(\delta,t) = T_0\,,\quad -kdT/dy\big|_{y_\delta=\delta(t)} = 0 \tag{9}$$

Where T (K) is the temperature, y_δ (m) is the location in the virgin material, t (s) is the time. δ (m) is the thermal penetration depth of the virgin material, k (W/mK) is the thermal conductivity of the virgin material. So the temperature profile in the virgin material is found to be:

$$T - T_0 = (T_p - T_0)(1 - y_\delta/\delta)^2 \tag{10}$$

The bottom layer is the char, the residue that remains after the pyrolysis reaction is completed. In this region, the thermodynamic properties are those of the residual char, and the temperature profile is assumed to be linear, and considering the boundary condition:

$$T(0,t) = T_s(t)\,,\quad T(\delta_c(t),t) = T_p \tag{11}$$

Where, T_s (K) is the surface temperature of the char, δ_c (m) is the char layer depth, and y_{δ_c} (m) is the location in the char. So the temperature profile in the char is found to be:

$$T - T_p = (T_s - T_p)(1 - y_{\delta_c}/\delta_c) \tag{12}$$

The vaporization plane separates the virgin material from the char. Here the virgin material pyrolyses into volatile gases and char. In this plane the temperature is constant at T_p.

In the vaporization plane, the mass conservation equation is expressed as:

$$\rho v = \dot{m}_c'' + \dot{m}'' \tag{13}$$

Where ρ (kg/m^3) is the density of the virgin material, $v = d\delta_c/dt$ (m/s) is the speed of the pyrolysis plane, $\dot{m}_c''$ (kg/m^{2}s) is the mass gain rate of the char, and $\dot{m}''$ (kg/m^{2}s) is the mass loss rate of the virgin material. Using $\dot{m}_c'' = \rho_c v$ and $\phi = \rho_c/\rho$, Eq. 13 can be rewritten as:

$$\frac{d\delta_c}{dt} = \frac{\dot{m}''}{\rho(1-\phi)} \tag{14}$$

Where ρ_c (kg/m^3) is the density of the char, and ϕ is the char fraction.

The energy conservation equation is:

$$\rho v h_v(T_p) - (\dot{m}''_c h_c(T_p) + \dot{m}'' h_g(T_p)) = \dot{q}''_k - \dot{q}''_v \tag{15}$$

Where, h_v (J/kgK), h_c (J/kgK) and h_g (J/kgK) are the specific enthalpy possessed by the mass entering the control volume, the char and the volatiles left behind by the vaporization plane, respectively. $\dot{q}''_k$ (kW/m^2) and $\dot{q}''_v$ (kW/m^2) are the heat conduction into the virgin material and the heat conduction from the char, respectively. We define the heat of vaporization ΔH_v (J/kgK) as energy required to convert the virgin material to the char and the volatiles such that:

$$\Delta H_v = h_v - h_g + \frac{\phi}{1-\phi}(h_v - h_c) = L - c(T_p - T_0) \tag{16}$$

Where L (J/kg) is the heat of gasification, and c (J/kgK) is the specific heat of the virgin material. Using Eqs. 10, 12 and 13, Eq. 15 can be reduced to:

$$\frac{\dot{m}''}{1-\phi}\Delta H_v = (-2k\frac{T_p - T_0}{\delta}) - (-k_c\frac{T_s - T_p}{\delta_c}) \tag{17}$$

Where k_c (W/mK) is the thermal conductivity of the char.

In the virgin material, the energy conservation equation is expressed as:

$$\rho c \frac{d}{dt}\int_0^{\delta}(T - T_0)dy_{\delta} = \dot{q}''_k - \rho v c(T_p - T_0) \tag{18}$$

Applying the temperature profile as Eq. 10 and integrating yields:

$$\frac{\rho c}{3}\frac{d\delta}{dt} + \frac{\dot{m}'' c}{1-\phi} = \frac{2k}{\delta} \tag{19}$$

In the char, the conservation energy is expressed as:

$$\rho_c c_c \frac{d}{dt}\int_0^{\delta_c}(T - T_0)dy_{\delta_c} = (\dot{m}''_c c_c(T_p - T_0) + \dot{m}'' c_g(T_p - T_0) + \dot{q}''_r) - (\dot{q}''_v + \dot{m}'' c_g(T_s - T_0) + \varepsilon\sigma(T_s^4 - T_0^4) + h(T_s - T_0)) \tag{20}$$

Where c_c (J/kgK) is the specific heat of the char, and c_g (J/kgK) is the specific heat of the volatiles. $\dot{q}''_r$ (kW/m^2) is the incident radiation heat flux. Using the temperature profile as Eq. 12, Eq. 20 can be further rewritten as:

$$\frac{\rho_c c_c}{2}[\frac{d\delta_c}{dt}(T_s + T_p - 2T_0) + \delta_c\frac{dT_s}{dt}] + \dot{m}''[c_g(T_s - T_p) - \frac{\phi}{1-\phi}c_c(T_p - T_0)] = \dot{q}''_r - \varepsilon\sigma(T_s^4 - T_0^4) - h(T_s - T_0) - k_c\frac{T_s - T_p}{\delta_c} \tag{21}$$

From the above analysis, Eqs. 14, 17, 19 and 21 are the mathematical equations that

describe the integral pyrolysis model. These equations track the thermal penetration depth δ, the char layer depth δ_c, the surface temperature T_s, and the mass loss rate $\dot{m}''$. The initial conditions are δ_{c0} =0, $\dot{m}''_0$ =0, $T_{s0} = T_p$ and $\delta_0 = 2k(T_p - T_0)/(\dot{q}''_r - \varepsilon\sigma(T_p^4 - T_0^4) - h(T_p - T_0))$.

It is stated that the assumption of semi-infinite solid is adopted in the above model, and then the above solution is invalid as soon as the following critical time is reached: the time $t_{\delta+\delta_c}$ reaches the back face, i.e., $\delta + \delta_c \le l$, which is usually meet when the material is preheated. If $\delta + \delta_c > l$ and $\delta_c \le l$, Eqs. 14, 17, 21 and $\delta = l - \delta_c$ can be solved to track δ, δ_c, T_s and $\dot{m}''$. The initial conditions for δ_c, T_s and $\dot{m}''$ are obtained from the results at the end of pyrolysis phase of $\delta + \delta_c \le l$.

Numerical Solution Procedure

Once the computation of heat-up is complete for element i, element i and $i-1$ can be examined to determine whether the pyrolysis front is present between the elements. If both temperatures are below T_p, then the entire section is still undergoing heat-up. If both temperatures are above T_p, then the entire section is undergoing pyrolysis and the pyrolysis front must exist in some other section. If one element is above and the other element below T_p, then the front must be between the elements and we can estimate its location by taking an intercept of a straight line, connecting the temperatures of the two elements with T_p.

From the above descriptions of heat-up and pyrolysis models, they both have been reduced to a system of simultaneous ordinary differential equation of Eqs. 5 and 6 for the heat-up model, and Eqs. 14, 17, 19 and 21 for the pyrolysis model. However, the differential equations are coupled non-linearly and therefore the system is not easily solvable. From the numerical point of view the system of differential equations for this case is stiff. In addition, when $\theta_s = 0$ or $\delta = 0$ for the heat-up model, and $\delta_c = 0$ for the pyrolysis model, the systems are also singular. To overcome this difficulty, the solution of the heat-up and pyrolysis models would be got using a Runge-Kutta method for stiff problems, and a fully implicit method and special attention should be given to the solution procedure [8].

In the paper, grid and time step sensitivity analyses are performed to determine an appropriate number of cells to use within the solid mesh and an appropriate time step, considering the numerical accuracy and computational efficiency. The study is intended to reveal the mesh and time step sensitivity to the pyrolysis front and the heat release rate. As a test case, Test No. 15 of ceiling flame spread experiments in the next section was undertaken. For the grid sensitivity analysis, the results for these simulations demonstrate that the pyrolysis front and heat release rate calculated from meshes consisting of 180×90, 240×120 and 300×150 cells (2.4 m in length and 0.012 m in thickness) and with 1 s time step show little differences. For the time step sensitivity analysis, three time

steps of 0.5 s, 1.0 s and 2.0 s and 240×120 meshes were adopted to compare the numerical results of the pyrolysis front and the heat release rate. And the comparison results demonstrate that the pyrolysis front and the heat release rate calculated using the three time steps show little difference. As a result, in this paper, for the simulations presented below 240×120 meshes and 1s time step were selected.

COMPARISONS WITH EXPERIMENTAL DATA

Validation of the Pyrolysis Model

The heat-up model has been validated in Ref. [5]. And the presented pyrolysis model will be validated against the experimental data obtained for white pine specimens subjected to a 40 kW/m^2 heat flux in nitrogen atmosphere [9]. The properties of white pine used in this simulation are taken from the literature: ρ =700 kg/m^3, k =0.34 W/mK, $c = c_c$ =1150 J/kgK, k_c =0.20 W/mK, c_g =1040 J/kgK, ϕ =0.2, T_0 =300 K, ε =0.9, h =15 W/mK. The pyrolysis temperature of 603 K and the heat of gasification of 1.8 MJ/kg are estimated from the measured surface temperature history and mass loss history. Along the direction of the incident radiation, the 0.038 m thick sample is discretized into 380 meshes, and the time step is taken as 1 s. The comparison between numerical predictions and experimental data is based on the time history of mass loss rates and the temperature profile at three locations, the surface, 0.5 cm and 1.0 cm below the surface.

The curves of the predicted and measured mass loss rates as a function of time are depicted in Fig. 3a. As can be seen from Fig. 3a, there is very good qualitative agreement between the predicted mass loss rate and those measured. The quantitative agreement is also reasonable. The predicted peak mass loss rate value (0.00663 kg/m^{2}s) is in very good agreement with the measured value (approximately 0.00621 kg/m^{2}s). The numerical mass loss rate increases more rapidly than the measured values. These differences are probably due to the effects of moisture within the wood sample which are neglected in the presented pyrolysis model. After the peak mass loss rate is achieved, the mass loss rate begins to decrease due to heat absorption of the char layer and enhanced surface reradiations which results from the high temperature at the char surface. During this decrease, the model predicts a smoother decline in the mass loss rate.

Figure 3b depicts the comparison of the predicted and measured temperature profiles at the top surface of the sample and at depths of 0.5 cm and 1.0 cm within the sample. As can be seen from Fig. 3b, the measured and the numerical top surface temperatures are in very good agreement. While the agreement between predicted and measured temperatures at the two deeper locations are not as good as at the surface, they at least maintain consistency. These differences are thought to be due to several simplifications within the pyrolysis model. As heat absorption by moisture is neglected in the presented pyrolysis model, more heat is conducted into the deeper portions of the wood. This causes the

predicted temperature to increase more rapidly than the measured values. Another major difference in the predicted and measured temperature occurs at the 0.5 cm depth during the late stage of pyrolysis. From the temperature history, it can be seen that this position is in the char layer during the late stage of pyrolysis. The deformation in the char layer and radiation flux penetrating through the char pores may affect the measured temperature. In addition, the experimental accuracy is another reason, because the deformations within the char layer may result in the thermocouple being closer to the surface. These factors may contribute to the discrepancies noted at the 0.5 cm and 1.0 cm depth measuring location.

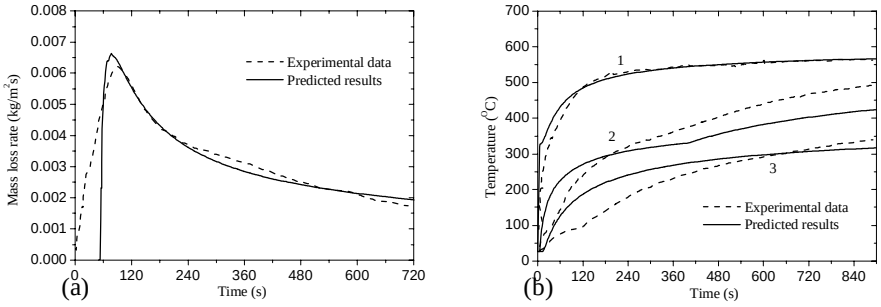

Fig. 3. Comparisons of predicted results including (a) the mass loss rate, (b) the temperature profiles: 1, at top surface; 2, at 0.5cm depth; 3, at 1.0cm depth with experimental data.

Comparisons with the Ceiling Flame Spread Experimental Data

In this section, the above model for the ceiling flame spread is compared with a set of experimental results produced as part of a series of experiments conducted by Hasemi and Yokobayashi [2-3]. The experimental detail can be found in Ref. [2].

The experimental conditions and data, and predicted results are shown in Table 1. $\dot{q}_e''$ was the external heat flux from the radiant panels. T_b was the surface temperature at the ignition time of the burner. $\dot{Q}_b$ was the heat release rate from the burner; the numbers outside the parentheses are measured with oxygen consumption method, and those in the parentheses are based on the assumption of complete combustion. x_{p0} was defined as $0.4\,L_f$, the area in which incident heat flux from the burner was nearly uniform [2]. L_f was the flame length only extended from the burner. x_{poff} was determined from the ultimate burn pattern and was defined as the weight average of the maximum distance and sidewall of the charred surface with crack. $\dot{Q}'_{mat_{\max}}$ was the peak heat release rate per unit width of material.

The properties of MDF used in this simulation are taken from the literatures. ρ =700 kg/m^3, T_p =653 K, $k = k_c$ =0.16 W/mK, $c = c_c$ =5545 J/kgK, c_g =1040 J/kgK, ϕ =0.1, T_p =653 K, T_0 =300 K, L =2.0 MJ/kg, ε =1.0, h =2.1 W/m^{2}K, χ =0.9, H_c =19.5 MJ/kg. The initial conditions of the heat-up model would be changed as

$\delta_0 = 2k(T_b - T_0)/\dot{q}_e''$ and $\theta_{s0} = T_b - T_0$. And the initial condition for the pyrolysis model is $\delta_0 = 2k[(T_p - T_b)/(\dot{q}_e'' + \dot{q}_f'') + (T_b - T_0)/\dot{q}_e'']$. The meshes of 240× 120 (2.4 m in length and 0.012 m in thickness) and the time step of 1s are adopted in this simulation.

Table 1. Experimental conditions and data, and predicted results.

Test No.	$\dot{q}_e''$ (kW/m^2)	T_b (^{o}C)	$\dot{Q}_b$ (kW)	x_{p0} (m)	Experimental data		Predicted results	
					x_{poff}/x_{p0}	$\dot{Q}'_{mat_{\max}}$ (kW/m)	x_{poff}/x_{p0}	$\dot{Q}'_{mat_{\max}}$ (kW/m)
4	6.56	157.5	7.3(10)	0.24	4.65	75.9	5.17	59.46
5	5.59	187.9	7.3(10)	0.24	5.81	106.6	4.96	82.25
6	5.42	155.5	7.3(10)	0.24	4.17	67.8	4.63	59.53
7	5.38	129.2	7.3(10)	0.24	4.13	60.9	4.25	41.07
8	5.38	121.5	10.8(15)	0.33	4.01	82.8	3.85	44.31
9	5.38	125.4	13.8(20)	0.43	3.56	83.1	3.58	54.60
10	3.94	120.8	7.3(10)	0.24	4.06	55.3	3.75	40.21
11	6.60	183.6	7.3(10)	0.24	5.84	102.0	5.67	82.13
12	5.37	123.3	10.8(15)	0.33	3.79	73.7	3.85	46.51
13	5.41	151.3	7.3(10)	0.24	4.64	63.0	4.54	55.83
14	5.37	122.6	10.8(15)	0.33	4.25	65.0	3.85	45.66
15	6.66	204.5	7.3(10)	0.24	6.97	105.0	8.33	102.48
16	6.61	185.3	4.3(5)	0.17	8.65	99.0	6.06	67.06
18	3.99	139.0	7.3(10)	0.24	3.66	45.0	3.63	38.55
19	8.76	207.0	4.3(5)	0.17	10.36	104.3	9.53	98.18

In the Table 1, it is clear that there is reasonably good agreement between experimental data and predicted results. For the predicted and measured x_{poff}/x_{p0}, the most discrepancy reaches 29.9% of Test No. 16, and the least discrepancy is 0.56% of Test No. 9. One of important reasons for this is that the ceiling flame spread is in two-dimension in the width way because of the stagnant progress of charred surface near the sidewalls due to the water cooling of the copper soffits. It should be noted that the predicted $\dot{Q}'_{mat_{\max}}$ are always lower than the experimental data. This shows that the presented ceiling flame spread model underestimates the heat release rate. The reason for this is probably from the underestimated heat flux exposure to the ceiling, and then the underestimated mass loss rate calculated from the pyrolysis model.

Figure 4 are the comparisons of the predicted results including (a) the flame length and the pyrolysis front, (b) the heat release rate per unit width with experimental data of Test No. 15, taken as an example. Time is counted from the start of preheating, i.e., 692 s. In this presentation of experimental data, it was assumed that arrival of the pyrolysis front was indicated by the surface temperature arriving at the ignition temperature of MDF, 380^{o}C. The experimental flame lengths during growing fires were the ultimate location of the flame tips on video tape at each time step. The heat release from the burner was removed from this presentation. As can be seen in Fig. 4a, the predicted flame length and

pyrolysis front compare fairly well with experimental data. Before the pyrolysis process, the predicted flame length is constant because only the burner, which is constant, contributes it. Otherwise, for the experiments, it needs time to stabilize the flame, and so the experimental flame length increases with time at the beginning stage. After the peak flame length is achieved, it decreases due to no enough gasified volatiles for enhancement of the flame, which results in the stoppage of the pyrolysis front. The predicted heat release rates per unit width also compare reasonably well with experimental data in Fig. 4b. Only little fewer predicted values exist. And the predicted heat release rate per unit width increases more rapidly than the measured values. The difference is thought to be due to the simplifications within the pyrolysis model, i.e., the neglected moisture in the material.

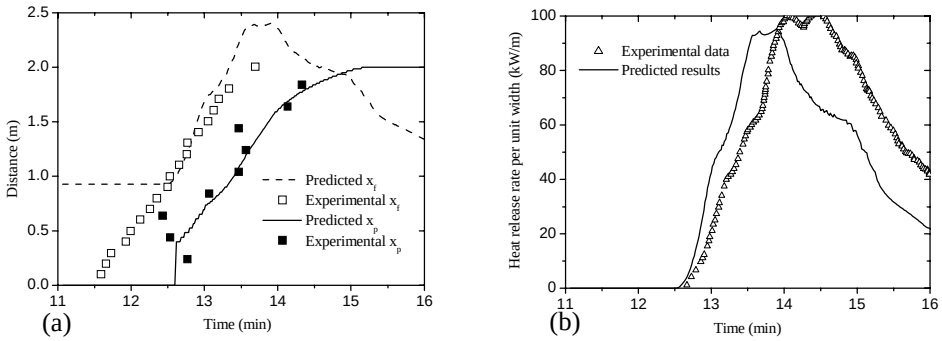

Fig. 4. Comparisons of predicted results including (a) the flame length and the pyrolysis front, (b) the heat release rate per unit width with experimental data.

CONCLUSIONS

A numerical model for ceiling flame spread beneath a combustible board is developed. This model consists of a one-dimensional ceiling flame spread model coupled with a one-dimensional pyrolysis model. The pyrolysis model is validated against the experimental data from the literature. The existing experimental data (the ceiling flame spread beneath medium density fibreboard (MDF)) are used for comparison to validate the presented model. The main conclusions are listed as follows: (1) Through comparing with experimental data, the presented integral pyrolysis model predicts the reasonably accurate mass loss rate---the primary purpose of pyrolysis models; (2) The numerical results obtained from the presented model are consistent with the ceiling flame spread experimental tests. Thus the presented model is appropriate for modeling ceiling flame spread; (3) The presented model underestimates the heat release rate. The reason for this is probably from the underestimated heat flux exposure to the ceiling, and then the underestimated mass loss rate calculated from the pyrolysis model; (4) It should be noted that the numerical results presented here are dependent on material properties which are estimated from experimental data, such as the pyrolysis temperature and the heat of

gasification. This is a feature common to all models using the pyrolysis temperature concept; (5) It is indicated that the presented numerical model can be used to model upward flame spread since the spread mechanism of the ceiling flame is the same as that of the upward flame; are both the concurrent flame spread. In addition, it would be useful to extend the modeling flame spread from wall to ceiling; and (6) The presented model probably predicts better the behaviors "fire retarded" charring materials since in general wood materials develop better char when they are fire retardant.

ACKNOWLEDGMENTS

The authors would like to acknowledge the support provided by the Japan Society for the Promotion Science Postdoctoral Fellowship (Grant No. 03246).

REFERENCES:

[1] Park, H.J., "An Investigation into Mysterious Questions Arising from the Daegu Underground Railway Arson Case through Fire Simulations and Small-scale Fire Tests," *Proceedings of the Sixth Asia-Oceania Symposium of Fire Science and Technology*, Daegu, Korea, 2004, pp. 1-27.

[2] Hasemi, Y., Yoshida, M., Yokobayashi, Y., and Wakamatsu, T., "Flame Heat Transfer and Concurrent Flame Spread in a Ceiling Fire," *Fire Safety Science—Proceedings of the Fifth International Symposium*, International Association for Fire Safety Science, 1997, pp. 379-390.

[3] Yokobayashi, Y., *Modeling of Heating Condition in Fire Safety Engineering*, Master Dissertation, Tokyo University of Science, 1995 (In Japanese).

[4] Saito, K., Quintiere, J.G. and Williams, F.A., "Upward Turbulent Flame Spread," *Fire Safety Science—Proceedings of the First International Symposium*, International Association for Fire Safety Science, 1985, pp. 75–86.

[5] Delichatsios, M.M., Mathews, M.K., and Delichatsios, M.A., "An Upward Fire Spread and Growth Simulation," *Fire Safety Science—Proceedings of the Third International Symposium*, International Association for Fire Safety Science, 1991, pp. 207–216.

[6] Baroudi, D., "A Discrete Dynamical Model for Flame Spread over Combustible Flat Solid Surfaces Subject to Pyrolysis with Charring---an Application Example to Upward Flame Spread," *Fire Safety Journal*, 2003, 38: 53-84.

[7] Zicherman, J.B. and Williamson, R.B., "Microstructure of Wood Char, Part II: Fire Retardant Treated Wood," *Wood Science & Technology*, 1982, 16: 19-34.

[8] Shapine, L.F., *Numerical Solution of Ordinary Differential Equations*, Chapman and Hall, New York, 1994.

[9] Kashiwagi, T., Ohlemiller, T.J. and Werner, K., "Effects of External Radiant Flux and Ambient Oxygen Concentration on Nonflaming Gasification Rates and Evolved Products of White Pine," *Combustion and Flame*, 1987, 69: 331-345.